

# Large-Area Characterization of Urban Morphology—Mapping of Built-Up Height and Density Using TanDEM-X and Sentinel-2 Data

Christian Geiß <sup>1</sup>, Member, IEEE, Tobias Leichte <sup>2</sup>, Michael Wurm <sup>3</sup>, Patrick Aravena Pelizari, Ines Standfuß, Xiao Xiang Zhu <sup>4</sup>, Senior Member, IEEE, Emily So, Stefan Siedentop, Thomas Esch, and Hannes Taubenböck <sup>5</sup>

**Abstract**—In this paper, we establish a novel multistep procedure for morphologic characterization of built environments in terms of built-up height and density. We rely on elevation measurements from the TanDEM-X mission (TDM) and multispectral Sentinel-2 imagery. These earth observation systems feature a notable tradeoff between a fairly high spatial resolution and large-area coverage and, thus, allow for spatially continuous analysis of built environments around the globe. To this purpose, we follow an automated workflow that foresees the distinction of “built-up” and “non-built-up” areas by relying on the so-called Global Urban Footprint processor. This information is deployed within a tailored filtering procedure for the TDM digital surface model data to extract elevation information for built-up areas. Subsequently, the intra-urban land cover is mapped under consideration of Sentinel-2 imagery and serves as basis to compute built-up heights and densities. These two measures are finally combined for a morphologic characterization of the built environment on an ordinal scale of measurement. Empirical validation efforts are provided based on comparative analysis with respect to more than 3.2 million individual building geometries and affiliated height measurements from

cadastral data sources. The datasets cover the settlement areas of the capital cities and other major cities in Germany, England, and the Netherlands. The experimental results underline the capability for a morphologic characterization of built environments with viable accuracies.

**Index Terms**—Built-up density estimation, built-up height estimation, Sentinel-2, TanDEM-X, urban morphology.

## I. INTRODUCTION

CHARACTERIZATION of built environments for large areas is a challenging but crucial task for, e.g., monitoring change in the context of urbanization [1], [2], identifying specific settlement types [3], [4], analyzing population in a spatiotemporal manner [5], [6], evaluating the energy performance of different types of urban form [7]–[11], assessing vulnerability and risks with respect to natural hazards [12], [13], and quantifying urban heat islands [14], [15], among others.

To address the aforementioned applications, earth observation (EO; a table with all abbreviations used in this paper can be found in the Appendix) data were already identified as a valuable source of information. Regarding the *spatial resolution* properties, past studies frequently relied on digital surface models (DSMs) (from, e.g., LiDAR measurements) and optical imagery (from, e.g., WorldView, GeoEye, etc.) with a very high spatial resolution (VHR) to resolve and analyze the comparable small objects of built environments such as buildings (e.g., [16]–[18]). However, the deployment of VHR data hampers utilization capabilities due to availability, economic costs, as well as processing requirements for large areas. When aiming at spatially continuous analyses and assessment approaches, which are applicable for large areas such as nations, continents, or even the globe, those kinds of data still represent a clear limitation nowadays.

However, especially recent EO systems internalize a remarkable tradeoff between a fairly high spatial resolution and large-area coverage. In particular, the TanDEM-X mission (TDM), which is a spaceborne radar interferometer, delivers a global DSM with an unprecedented pixel spacing of 0.4 arcseconds ( $\sim 12$  m) [19], [20]. Regarding optical imagery, ESA’s Sentinel-2 satellites [21] deliver imagery with a spatial resolution of 10 m for the bands covering visible light and near infrared. Sentinel-2 data are provided free of charge to the public via a data hub.

Manuscript received January 22, 2019; revised April 9, 2019; accepted May 12, 2019. Date of publication June 24, 2019; date of current version September 16, 2019. This work was supported in part by the German Federal Ministry for Economic Affairs and Energy’s initiative “Smart Data—innovations from data” under grant agreement: “smart data for catastrophe management (sd-kama, 01MD15008B),” in part by the European Research Council (ERC) under the European Union’s Horizon 2020 research and innovation program under Grant 714087 - So2Sat, in part by the BMBF under Grant 03G0876, and in part by the German Research Foundation (DFG) for Project “Where are the jobs? Stadregionale Zentrenstrukturen im internationalen Vergleich” under Grant TA 800/6-1 and Grant SI 932/12-1. The work of C. Geiß was supported by the Helmholtz Association under Grant “pre\_DICT” (PD-305). (Corresponding author: Christian Geiß.)

C. Geiß, M. Wurm, P. Aravena Pelizari, I. Standfuß, T. Esch, and H. Taubenböck are with the German Remote Sensing Data Center (DFD), German Aerospace Center (DLR), Weßling 82234, Germany (e-mail: christian.geiss@dlr.de; michael.wurm@dlr.de; patrick.aravenapelizari@dlr.de; ines.standfuss@dlr.de; thomas.esch@dlr.de; hannes.taubenboeck@dlr.de).

T. Leichte was with the Company for Remote Sensing and Environmental Research (SLU), Munich 81243, Germany. He is now with the German Remote Sensing Data Center (DFD), German Aerospace Center (DLR), Weßling 82234, Germany (e-mail: tobias.Leichte@dlr.de).

X. X. Zhu is with the Remote Sensing Technology Institute (IMF), German Aerospace Center (DLR), Weßling 82234, Germany (e-mail: xiao.zhu@dlr.de).

E. So is with the Department of Architecture, Cambridge University Centre for Risk in the Built Environment (CURBE), University of Cambridge, Cambridge CB2 1PX, U.K. (e-mail: ekms2@cam.ac.uk).

S. Siedentop is with the ILS – Research Institute for Regional and Urban Development, Dortmund 44135, Germany (e-mail: stefan.siedentop@ils-forschung.de).

Color versions of one or more of the figures in this paper are available online at <http://ieeexplore.ieee.org>.

Digital Object Identifier 10.1109/JSTARS.2019.2917755

Given those properties, here, we complementarily employ data from both systems for large-area characterization of built environments.

Regarding *thematic resolution* properties, past studies primarily characterized built environments with respect to building types [22]–[27], or urban structure types (i.e., distinctive and homogeneous assemblages of land cover/land use elements) [28], [29] with a high level of semantic detail based on sufficient and properly encoded prior knowledge. This allows inferring empirical relationships for predefined and specific semantic levels using supervised learning techniques (e.g., discriminate between buildings/zones of residential, commercial, and industrial usage).

In contrast to those approaches, we aim to quantitatively characterize built environments without the incorporation of prior knowledge and *a priori* determination of thematic classes according to specific semantics. This is done to allow for consistent and automated large-area analysis. Additionally, in this way, we bypass local idiosyncrasies (e.g., different settlements may contain different building types and similar types might feature a different physical appearance in various settlements, which is shaped by natural and cultural factors). With it, we aim for a consistent and objective statistical description of settlements. Thus, such a quantitative characterization can be transferred into thematic classes *a posteriori* and allows also for a targeted collection of *in situ* knowledge for dedicated applications.

Recently, Heinzel and Kemper [16] established an unsupervised workflow based on VHR airborne multispectral imagery for a joint description of settlements according to maximum building size, heterogeneity of the building size, and built-up density. To this purpose, they use operations from mathematical morphology [30] on the imagery. Based on spaceborne multispectral imagery, Zhang *et al.* [31] estimate building density in a supervised manner using advanced regression techniques. González-Aguilera *et al.* [17] deploy VHR LiDAR data for derivation of geometric information (heights, areas, and volumes) and urban density attributes (building coverage ratio and floor area ratio) of buildings, land lots, and urban units. More thematically guided, Taubenböck *et al.* [18] produce three-dimensional building models in level of detail 1 (LoD-1) resolution (i.e., buildings are represented by extruded footprints) [32] by using a combination of VHR optical imagery and auxiliary data sources (such as geo-tagged ground photos or *in situ* surveys). Based on this data they characterize spatial patterns of buildings in terms of density, orientation, and heterogeneity of alignment and compute individual building size and height for analysis of so-called “Arrival Cities.”

However, as mentioned before and in contrast to previous works, we jointly exploit DSM data from the TDM and Sentinel-2 multispectral imagery to characterize urban morphology. These data sets feature a global coverage and allow for a unique mapping of urban morphology for large areas. At the same time, the spatial resolution properties of the data hamper analyses on individual building level. The pixel spacing of 0.4 arcseconds for the TDM data and 10 m for the multispectral

Sentinel-2 imagery can exceed the extent of the objects of interest (i.e., buildings). As a consequence, we work on an aggregated spatial level, i.e., we establish spatial processing units in terms of rectangular grid cells to compute morphologic properties of built-up structures. Thereby, we focus our work on the most constituent properties of urban morphology, namely, built-up height and density. The latter represents one of the most important descriptive, explanatory, as well as normative measures in urban research [33], [34]. In addition to that, the presence of buildings adds a third dimension to be considered among the environmental relationships found in urban areas. Thus, the vertical dimension of built environments must be taken into account to enable a holistic assessment [35]. Consequently, the measure built-up height is also incorporated in our approach. These two measures describing urban morphology are also in line with and can support generic mapping schemes such as the local climate zone (LCZ) concept [36], which aims to classify natural and urban landscapes into categories based on climate-relevant surface properties. Thus, built-up height and density are determinant properties for categorizing urban landscapes [37], [38].

To address the aforementioned considerations, we establish a workflow to estimate built-up height and density for spatial processing units. These two measures are finally combined for a morphologic characterization of the built environment on an ordinal scale of measurement, which represents combinations of *low*, *medium*, and *high* built-up heights and densities. We built upon our initial works regarding this subject [39]. However, the contributions of this paper can be considered as follows.

- 1) A novel workflow is proposed to estimate built-up height and density automatically and derive corresponding ordinally scaled classes with respect to spatial processing units thereof. In particular, we first build upon the so-called Global Urban Footprint (GUF) processor [40]. This procedure provides binary information on “built-up” and “non-built-up” areas on a global scale. It is deployed within a filtering procedure on the TDM DSM data to extract the required elevation information solely within built-up areas. Thereby, intra-urban water bodies are also automatically excluded. Subsequently, intra-urban land cover (LC) (i.e., LC within “built-up” areas as indicated by the GUF data set) is consecutively mapped according to the thematic classes “intra-urban vegetation”, “elevated built-up”, and “residual intra-urban LC.” This information serves as basis to compute built-up heights and densities.

- 2) Exhaustive validation efforts are carried out in an original manner. We compute relevant accuracy measures based on comparisons with LoD-1 building models from areas which cover ten large cities in three countries in Europe (i.e., Berlin, Hamburg, Munich, Cologne, Frankfurt, Stuttgart, London, Amsterdam, Rotterdam, and The Hague). As such, the main objective of this study is to evaluate the performance and overall suitability of automatic computations of built-up heights and densities from TDM and Sentinel-2 data for an efficient spatial differentiation of entire metropolitan regions into areas of *low*, *medium*, and *high* built-up height and density.

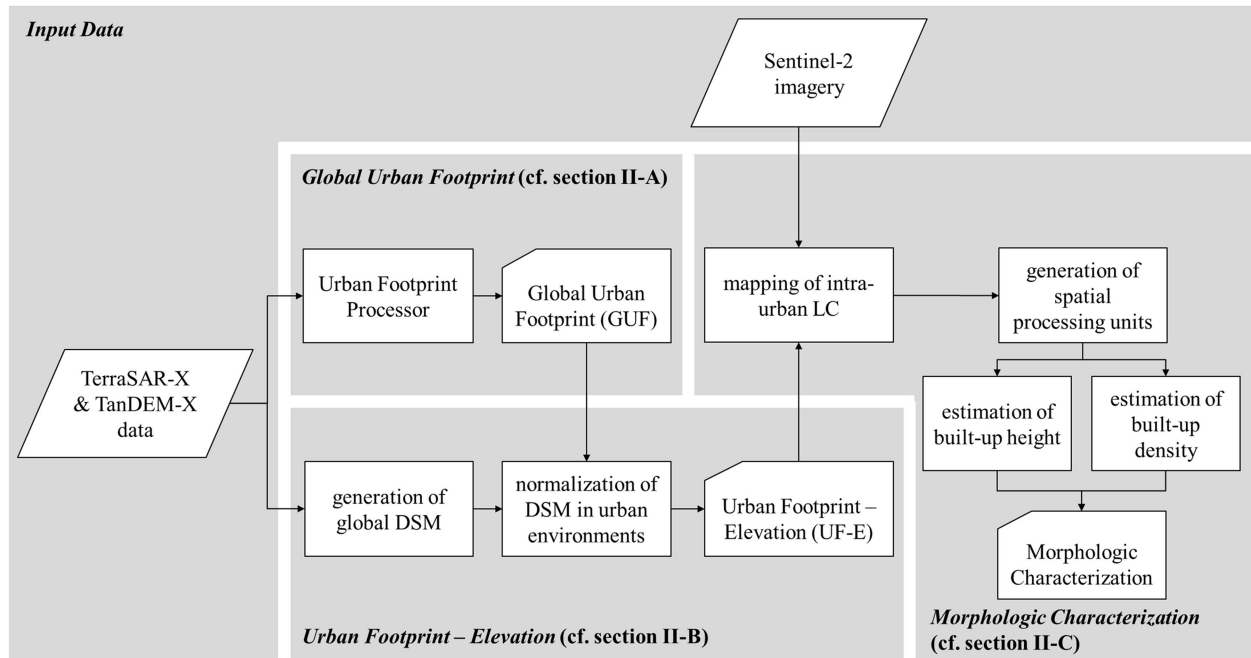


Fig. 1. Flowchart of the approach for characterization of urban morphology in terms of built-up height and density.

The remainder of the paper is organized as follows. Section II gives an overview of developed methods and Section III is used to present the deployed data sets and explain the experimental setup. Section IV provides experimental results and validation efforts. Concluding remarks and an outlook are given in Section V.

## II. PROPOSED METHODOLOGY

A flowchart of the approach is given in Fig. 1. It builds upon data from the TDM and Sentinel-2 and consists of three main consecutive data processing modules. The first module builds upon the GUF processor, which is used to discriminate “built-up” and “non-built-up” areas in a binary manner (Section II-A). The second module extends this binary description in terms of elevation information. To this purpose, elevation information in built environments is retrieved automatically using the DSM which was derived globally from the TDM (Section II-B). The third module contains the calculation of built-up height and density, which subsequently constitutes the generic morphologic characterization of built environments (Section II-C).

### A. Global Urban Footprint

To efficiently constrain data processing and analysis on built environments, we build upon the outcomes of a fully automated image analysis procedure, which discriminates “built-up” and “non-built-up” LC. Based on the TDM, which collected data sets of high resolution synthetic aperture radar (SAR) images, built-up areas can be extracted with an unprecedented spatial detail on a global scale. This is due to the circumstance that built-up areas show a distinct small-scale heterogeneity of local

backscatter in the imagery. As such, the image analysis procedure foresees the computation of the speckle divergence as texture measure which is defined as the ratio between the local standard deviation and local mean of the backscatter computed in a defined local neighborhood. The speckle divergence will take very high values over built-up areas due to the occurrence of bright backscatter (as induced by, e.g., double bounce effects and direct reflections at buildings) in close spatial proximity to dark areas (as induced by e.g., shadows or specular reflections at smooth surfaces such as roads). Subsequently, the speckle divergence is jointly deployed with the original backscattering amplitude for classification of built-up areas. To this purpose, the classification procedure first implements thresholds derived from image statistics of the amplitude and texture data, respectively, to reliably identify image elements (i.e., pixels) of built-up areas. The identified image elements serve as labeled samples for learning one-class classification models based on Support Vector Domain Description to establish optimal model solutions for the individual image scenes [40].

Generally, the data set does not contain spatially and thematically exact measurements of individual urban objects, but provides a more abstract delineation of the physical man-made properties of cities (i.e., built-up areas). Finally, post-editing procedures ensure an overall absolute accuracy of about 85% [40], which underlines a reliable identification of built-up areas [41].

### B. Urban Footprint—Elevation

In combination with the GUF data set, the elevation measurements of the TDM are used to compute a normalized DSM (nDSM). Consequently, the latter comprises elevation information of objects above ground in built-up areas. To this purpose, a

digital terrain model (DTM) is derived first from the DSM with a so-called region growing-based progressive morphological filter procedure. This approach was first proposed by Geiß *et al.* [42] to address general challenges associated with the use of morphological filters in non-flat terrain and is intended to overcome particular challenges related to the spatial resolution of TDM data.

A detailed description of the underlying algorithms with pseudocode is provided in [42]. The procedure includes a multistep method using concepts of morphological image filtering, region growing, and interpolation techniques. It is based on the idea of progressive morphological filters, which aim to discriminate ground and nonground pixels in the DSM based on algebraic set operations. Such filters identify nonground pixels in the DSM by gradually increasing the size of a structuring element and applying iteratively an elevation difference threshold. After the identification of initial nonground pixels, here, potential nonground pixels are identified within each iteration and their similarity with respect to neighboring nonground pixels is assessed. Potential nonground pixels are finally labeled as nonground if they feature a high similarity to already identified nonground pixels. Thus, it is also made sure that intra-urban water bodies are excluded from the analysis using the TDM water indication mask, which is an automatically processed information layer included in the TDM DSM product [43].

After complete identification of nonground pixels, corresponding ground pixels are subsequently interpolated to a DTM using an exact interpolation technique. Finally, the DTM is subtracted from the DSM to receive the final nDSM in built environments [i.e., Urban Footprint – Elevation (UF-E)].

### C. Morphologic Characterization

The calculation of built-up height and density is based on an intra-urban LC map. To establish the LC map, the UF-E data set is combined with Sentinel-2 imagery. The latter serves for computing the Normalized Difference Vegetation Index (NDVI) [44]. The NDVI internalizes different reflection properties of vegetation in the red and NIR band, respectively. High numerical values indicate photosynthetically active vegetation. In this manner, it can be noted that the GUF algorithm relies on distinctive SAR-related backscatter mechanisms of vertical, unpenetrable structures (i.e., built-up structures), and thus, the data set does not contain larger fractions of vegetation (e.g., urban forests [45]) [46]. However, small vegetation patches are automatically excluded before further processing by adaptively thresholding NDVI values of Sentinel-2 imagery using Otsu’s method. The method searches for a threshold to separate two classes with minimum intra-class variance, i.e., maximum inter-class variance [47]. In this method, the group with higher NDVI values corresponds to intra-urban vegetation, whereas the group with lower NDVI values contains the remaining LC classes. Subsequently, elevated built-up areas are discriminated from residual intra-urban LC. This is done to prune intra-urban LC which cannot represent the objects of interest (i.e., buildings). Thus, we assume that pixels within the residual settlement area (i.e., built-up areas without intra-urban vegetation as identified in the

previous processing step) represent elevated built-up areas if they exceed a certain height threshold  $\Theta$  in the associated UF-E model.

The actual calculation of built-up height and density as well as their joint representation for final morphologic characterization is provided on spatial processing units. This is done to allow for a robust representation of extracted height values based on a statistical measure of central tendency (i.e., a quantile  $Q_n$ ) and computing densities from the binary elevated built-up area pixels. In addition, in this way, robust comparisons to reference data with different resolution properties can be achieved. Here, rectangular grid cells of size  $a \times a$ , based on the arrangement of the image elements of the Sentinel-2 data, are used to rely on comparable spatial entities which are ubiquitously available throughout built environments (alternatively, irregular spatial processing units such as superpixels from an image segmentation procedure [29] or street blocks generated from geospatial vector data [25] can be exploited). Consequently, built-up height and density per grid cell are calculated as follows:

$$\text{built-up height}_{\text{grid cell}} = Q_n(n\text{DSM}_{\text{elevated built-up}}) \quad (1)$$

where  $Q_n$  is the aggregation function (i.e., statistical measure of central tendency) and  $n\text{DSM}_{\text{elevated built-up}}$  are the numerical height values contained in the UF-E model for the pixels labeled as LC class “elevated built-up”

$$\text{built-up density}_{\text{grid cell}} = \frac{A_{\text{elevated built-up}}}{A_{\text{built-up}}} \quad (2)$$

where  $A_{\text{elevated built-up}}$  is the area covered by pixels labeled as LC class “elevated built-up” and  $A_{\text{built-up}}$  is the area covered by pixels labeled as “built-up” (i.e., GUF).

Finally, estimated built-up height and built-up density values per grid cell are joined to nine morphologic classes, which represent combinations of *low*, *medium*, and *high* built-up heights and densities.

## III. DATA SETS AND EXPERIMENTAL SETUP

### A. DSM Data From TanDEM-X

As mentioned earlier, the TDM elevation model can be dominantly regarded as a DSM, especially when analyzing built environments as in this study. Only few surfaces such as ice, snow, or vegetation can be penetrated by the X-band SAR signal [48]. Comparisons to ICESat data underline the high quality of elevation measurements, which feature less than one meter deviation in absolute vertical accuracy for surfaces other than highly vegetated areas or snow-/ice-covered regions. [49]. Overall, 14 TDM tiles ( $1^\circ$  by  $1^\circ$ ) with a spatial resolution of 0.4 arcseconds (i.e.,  $\sim 12$  m) were processed to consistently cover the settlement areas of all ten considered cities.

### B. Multispectral Imagery From Sentinel-2

The multispectral Sentinel-2 imagery were subject to atmospheric corrections within the Sentinel Application Platform [50] using the Sen2Cor module [51] to provide level 2A products. We deploy Sentinel-2’s red (665 nm) and nir (842 nm)

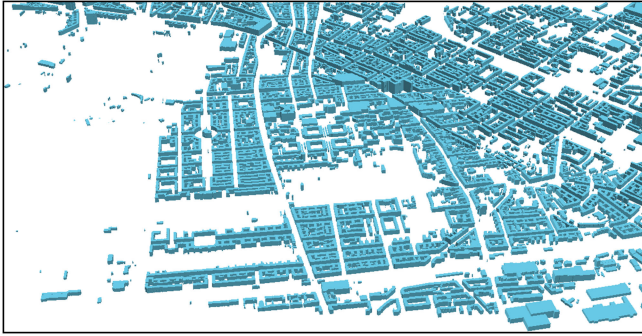


Fig. 2. LoD-1 model for a subset of the city of Berlin.

bands, which feature a spatial resolution of 10 m, for computation of NDVI values. The imagery for the different cities was acquired in autumn and winter of the years 2014–2016. The dates were chosen to reduce the effect of vegetation on the intra-urban LC classification since intra-urban vegetation frequently obscures underlying built-up structures [52].

### C. Reference Data

As reference data sets, we incorporated LoD-1 building models comprising more than 3.2 million building geometries and affiliated height measurements, which are based on cadastral information for the cities in Germany [53] and the Netherlands [54], as well as edited OpenStreetMap data for the city of London [4]. Fig. 2 illustrates the reference LoD-1 models for a subset of the city of Berlin (the subset corresponds also to the area which is shown in the zoom-in windows of Fig. 4). The building geometries were resampled and properly aligned to the image elements of the Sentinel-2 data for comparison. The resulting binary built-up mask was used for computation of built-up height and density per grid cell, whereas median height values (i.e.,  $Q_{50}$ ) were deployed for subsequent comparisons.

### D. Experimental Setup and Parameterization

The filter procedure for normalization of the DSM needs some free parameters to be fixed. The structuring element of the morphological filter must always exceed a building's outline to ensure extraction of all buildings present in the area under investigation. Consequently, the side length of the structuring element was determined empirically for the study areas according to the largest buildings present in the data. Additionally, an elevation difference threshold and a similarity constraint need to be determined. Both were set in accordance to previous experimental analysis, to enable a favorable tradeoff between decrease of omission errors and increase of commission errors when classifying ground pixels (i.e., 2.6 m for the elevation difference threshold and 1 m for the similarity constraint [42]). Besides, we derived a binary water mask with maximum extent from the water indication mask, which is provided with the TDM data, by selecting values from 3 to 127 (i.e., thresholds of TDM amplitude and coherence) [43]. Inverse distance weighting [55] with an adaptive neighborhood was deployed for interpolation

of identified ground pixels. The deployed GUF data sets feature a spatial resolution of 12 m. The obtained scene-specific NDVI thresholds, as determined with Otsu's method, are quite restrictive in classifying vegetation and range from 0.35 (Munich) to 0.46 (Cologne). We evaluated results as a function of different height thresholds for establishing the intra-urban LC map, i.e.,  $\Theta = \{>0 \text{ m}, 3 \text{ m}, 5 \text{ m}\}$ . In addition, we tested different aggregation functions for estimation of built-up height per grid cell. As described before, we represent height values of grid cells by quantiles  $Q_n$ . For a systematic evaluation, different deciles are tested, i.e.,  $Q_{50}$ ,  $Q_{70}$ ,  $Q_{90}$ . Previous experiments showed that built-up heights are in tendency underestimated [39]. This motivated us to also establish built-up height estimations using upper deciles in addition to the median to eventually balance likely underestimations. Regarding the edge length of grid cells, we evaluate results with respect to  $a = \{200 \text{ m}, 500 \text{ m}, 800 \text{ m}\}$ . Those values were found empirically to allow reflecting areas of homogeneous urban morphology in previous studies (e.g., [4], [34]). As described earlier, the measurements are finally combined within the defined nine morphologic classes. The thresholds for low, medium, and high built-up heights and densities were set according to numeric values, which are consistent with the values provided by the LCZ concept [36], i.e., a threshold of 0.2 for *low* built-up densities and 0.4 for *high* built-up densities was chosen, in conjunction with a threshold of 10 m for *low* built-up heights and 25 m for *high* built-up heights, respectively.

Statistical evaluation is carried out based on a set of accuracy measures. The accuracy of built-up height and density estimates is evaluated based on mean error (ME)

$$\text{ME} = \frac{1}{N} \sum_{i=1}^N (\hat{X}_i - X_i) \quad (3)$$

where  $\hat{X}_i$  is the numerical value per grid cell computed from the intra-urban LC map  $\hat{X}$ ,  $X_i$  is the numerical value per grid cell derived from the reference data  $X$ , and  $N$  is the number of grid cells. Thus, positive ME values (i.e.,  $\text{ME} > 0$ ) indicate an overestimation, whereas negative ME values (i.e.,  $\text{ME} < 0$ ) indicate an underestimation of built-up height and density estimates with respect to the reference. In addition, the mean absolute error (MAE) is computed analogously [56] to provide absolute deviation levels

$$\text{MAE} = \frac{1}{N} \sum_{i=1}^N (|\hat{X}_i - X_i|). \quad (4)$$

Regarding the final combination of computed built-up height and density within nine morphologic classes, we derived classification accuracy measures from a weighted confusion matrix to account for the ordinal scale of measurement, which prohibits the valid use of accuracy measures derived from a conventional confusion matrix [57]. Consequently, a deviation of one ordinal class (e.g., class “*low density – low height*” is confused with “*low density – medium height*”) is solely penalized with a weighting factor of 0.25, two classes are penalized with a factor of 0.5, three classes are penalized with a factor of 0.75, and higher deviations are fully penalized. For illustration, Fig. 3 shows the

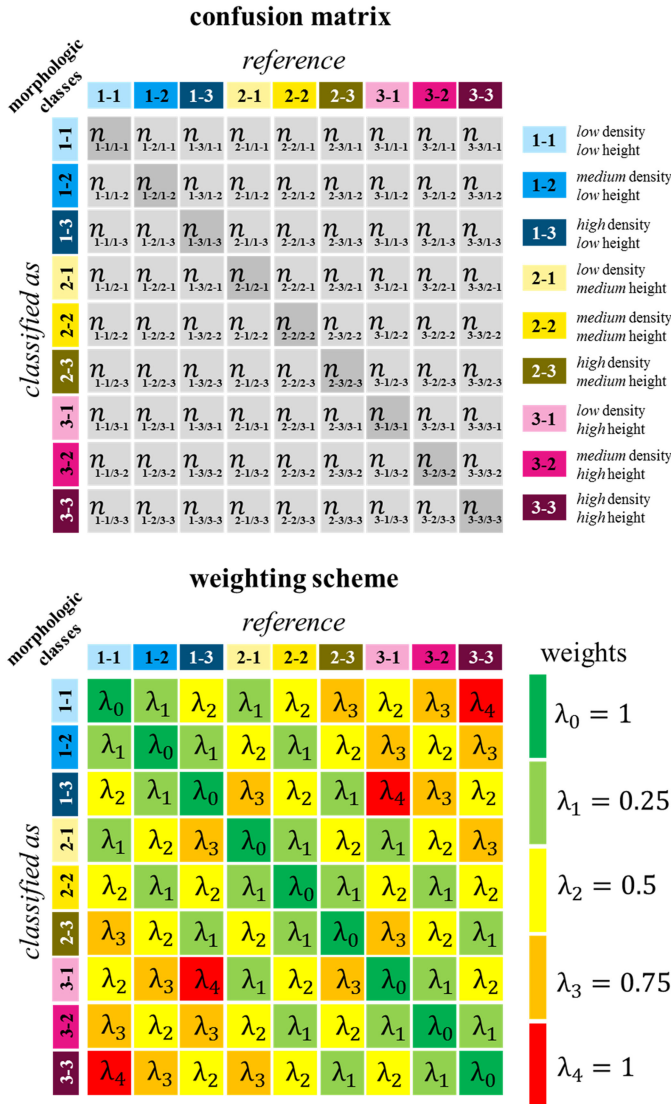


Fig. 3. Confusion matrix and weighting scheme with respect to the nine ordinal morphologic classes for computing a weighted confusion matrix.

weighting scheme for the number of instances  $n$  of the respective morphologic classes.

This scheme is multiplied with the unweighted confusion matrix, whereby the residual instances, i.e.,  $((1 - \lambda) * n)$  are added to the correctly classified instances of the respective class located at the diagonal of the matrix. To evaluate class-specific differences in accuracy, we derived user’s and producer’s accuracies from the weighted confusion matrix. In addition, the overall accuracy (OA) as well as  $\kappa$  statistics [58] were computed as global accuracy measures.

#### IV. EXPERIMENTAL RESULTS AND DISCUSSION

An exemplary visualization of the outcomes of the different data processing steps in terms of TDM DSM data with binary water mask, atmospherically corrected Sentinel-2 data, GUF, and UF-E for the city of Berlin, Germany, is provided in Fig. 4. In addition, the intra-urban LC map is also shown, which serves

as a basis to compute built-up height and density. The zoom-in window already allows inferring some fundamental properties of the respective data sets. The TDM DSM resolution of  $\sim 12$  m does not consistently allow reconstructing the individual building footprints. However, the built-up structures can be clearly depicted in the grayscale image representation of the DSM [see Fig. 4(a)]. To extract complementary information, multispectral Sentinel-2 imagery offers a suitable tradeoff between covering large areas and simultaneously capturing details of the built environment [see Fig. 4(b)]. The GUF data set accurately identifies “built-up” LC, whereby larger vegetation areas or bare soil patches between built-up areas are also correctly labeled as “non-built-up” [see Fig. 4(c)]. The intra-urban nDSM (i.e., UF-E) extends the thematic resolution of the GUF data sets by assigning a rational scaled elevation value, which also clearly allows identifying elevated objects of built environments [see Fig. 4(d)]. To further refine the spatial distinction of “built-up” and “non-built-up”, intra-urban vegetation areas are labeled under consideration of the multispectral imagery [see Fig. 4(e)]. Subsequent to that, the UF-E model is used to further distinguish between “elevated built-up” and “residual intra-urban LC” in the remaining areas ( $\Theta$  was set to 3 m in this visualization, which corresponds approximately to one floor [59]). Only pixels of the class “elevated built-up” and affiliated elevation values from the UF-E model are used for mapping built-up heights and densities and creating the morphologic classes.

##### A. Accuracy of Built-Up Height

Accuracy of built-up height estimations differentiated with respect to the nine morphologic classes is provided in Fig. 5. The morphologic classes were created based on the reference data sets of all ten considered cities. Results are presented as a function of different values for the height threshold  $\Theta$ , the aggregation function for estimation of built-up height per grid cell, and the size of the grid cells.

The ME reveals a systematic underestimation of built-up height estimations in relation to the reference data for all morphologic classes [see Fig. 5(a)]. Only some estimates based on restrictive values for  $\Theta$  (i.e.,  $\Theta = \{>3 \text{ m}, 5 \text{ m}\}$ ) provide overestimations predominately for morphologic classes with *low* built-up density. The MAE [see Fig. 5(b)] uncovers increasing height deviations with an increasing built-up height. This can be naturally related to the increasing range of numerical height values. In addition, areas which show a *high* built-up height in conjunction with a *low* built-up density are prone to layover and shadow effects, which prohibit capturing valid elevation measurements. However, height estimations feature lower error levels with an increasing built-up density. Generally, error levels can be balanced by choosing an appropriate aggregation function. Thus, the most progressive value considered in this study (i.e.,  $Q_{90}$ ) consistently provides most favorable error levels, which underline systematically low elevation values in the underlying TDM data in relation to the ground truth information. This relation also explains favorable error levels induced by restrictive  $\Theta$  values. Thus, only built-up areas are considered for height

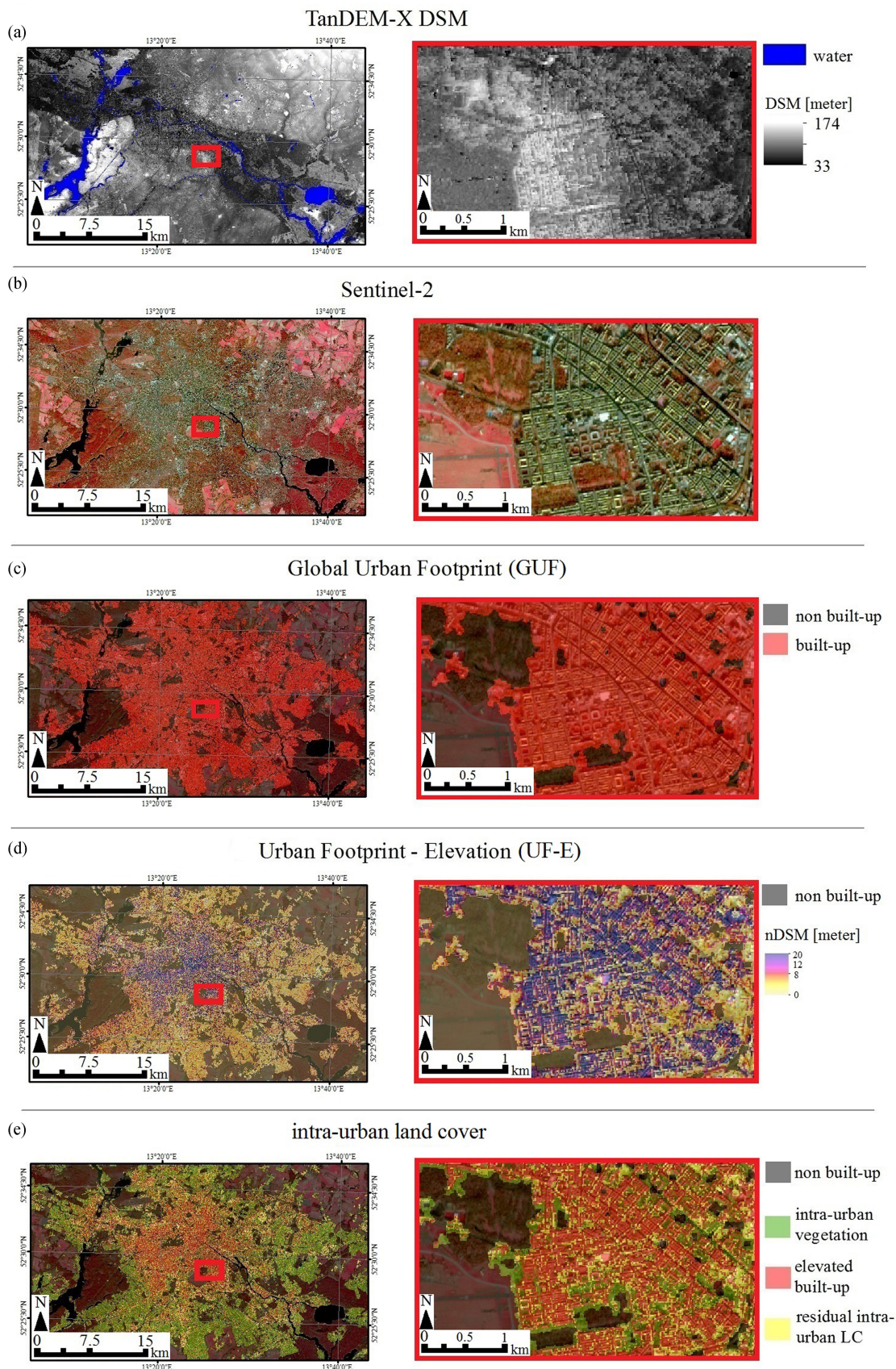


Fig. 4. Overview on the different data sets for the city of Berlin, Germany. (a) TDM DSM data with binary water mask. (b) Atmospherically corrected Sentinel-2 multispectral imagery in false-color representation. (c) GUF data set which discriminates “built-up” areas from “non-built-up” areas. (d) The UF-E model provides intra-urban elevation values. (e) Intra-urban LC map which discriminates three thematic classes.

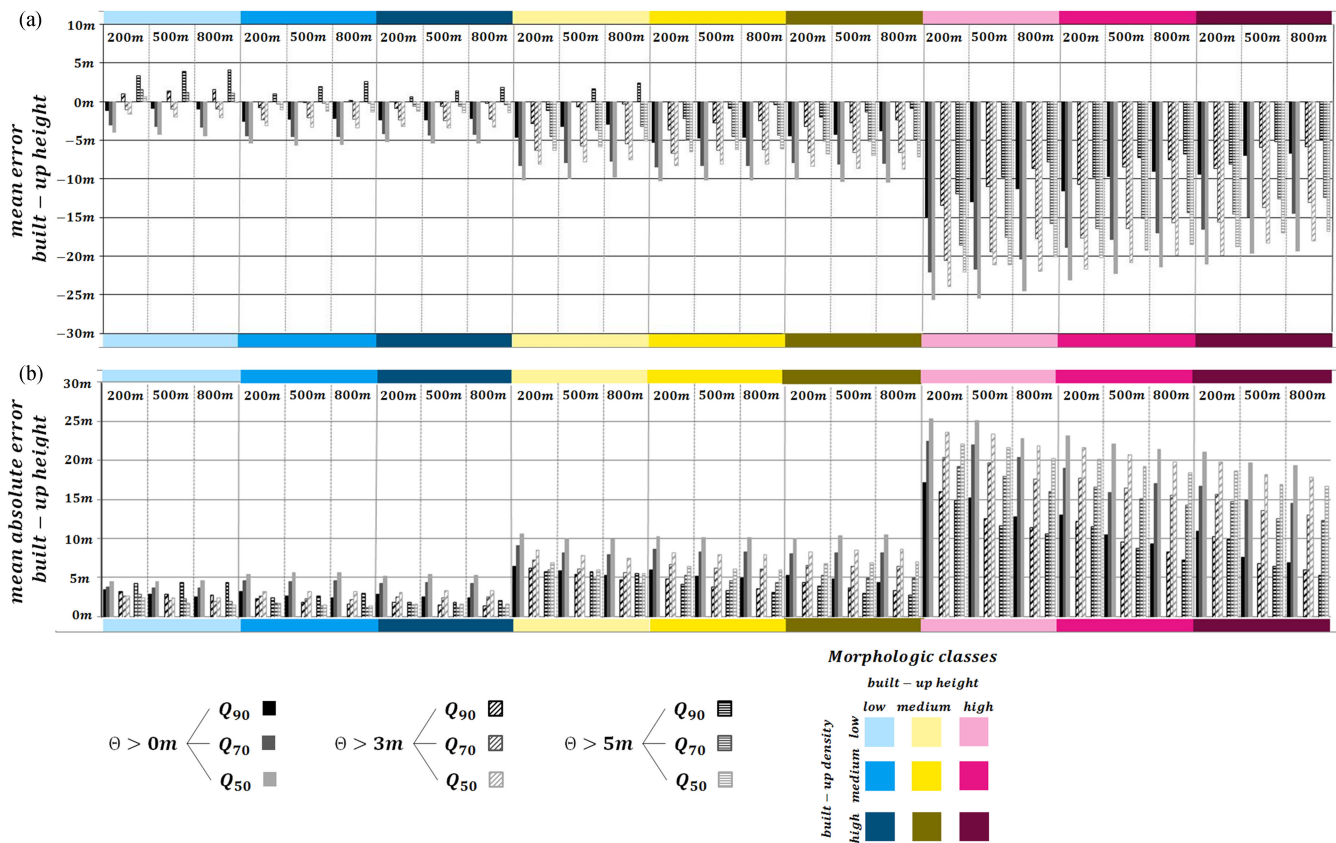


Fig. 5. Error measures for built-up height estimations. (a) ME and (b) MAE differentiated according to the nine morphologic classes and different values for the height threshold  $\Theta$ , the aggregation function for estimation of built-up height per grid cell, and the size of the grid cells.

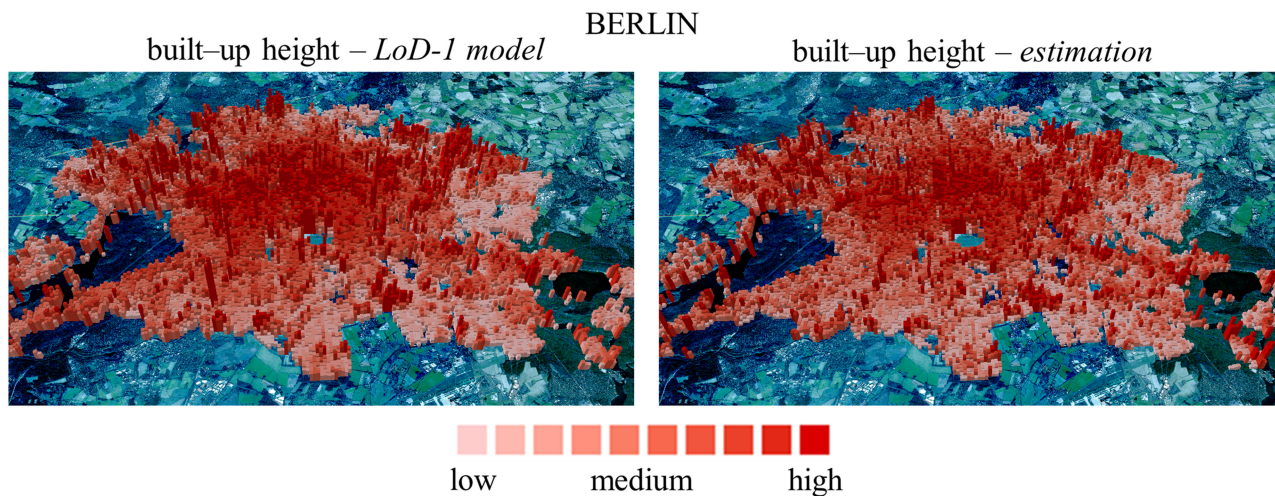


Fig. 6. Visualized built-up heights according to  $a = 200\text{ m}$  ( $\Theta = 3\text{ m}$  and height is represented by  $Q_{90}$  with respect to the *estimation*) for the example of Berlin, Germany. Color coding corresponds to deciles for the individual data sets and thus allows a relative spatial comparison; however, heights of bars correspond to absolute numerical values where numerical height values were superelevated 50 times.

estimation, which already exceed certain elevation values and, thus, provide progressive built-up height estimations. Overall, error levels based on favorable combinations of hyperparameters feature a deviation of less than one floor for built-up areas with *low* heights, one to two floors for *medium* high built-up

areas, and approximately two floors for *high* built-up areas if built-up structures are not overly sparse, which underline the viability of the approach. Finally, it can be noted that errors levels frequently decrease slightly with an increasing size of the grid cells, which can be related to averaging effects.

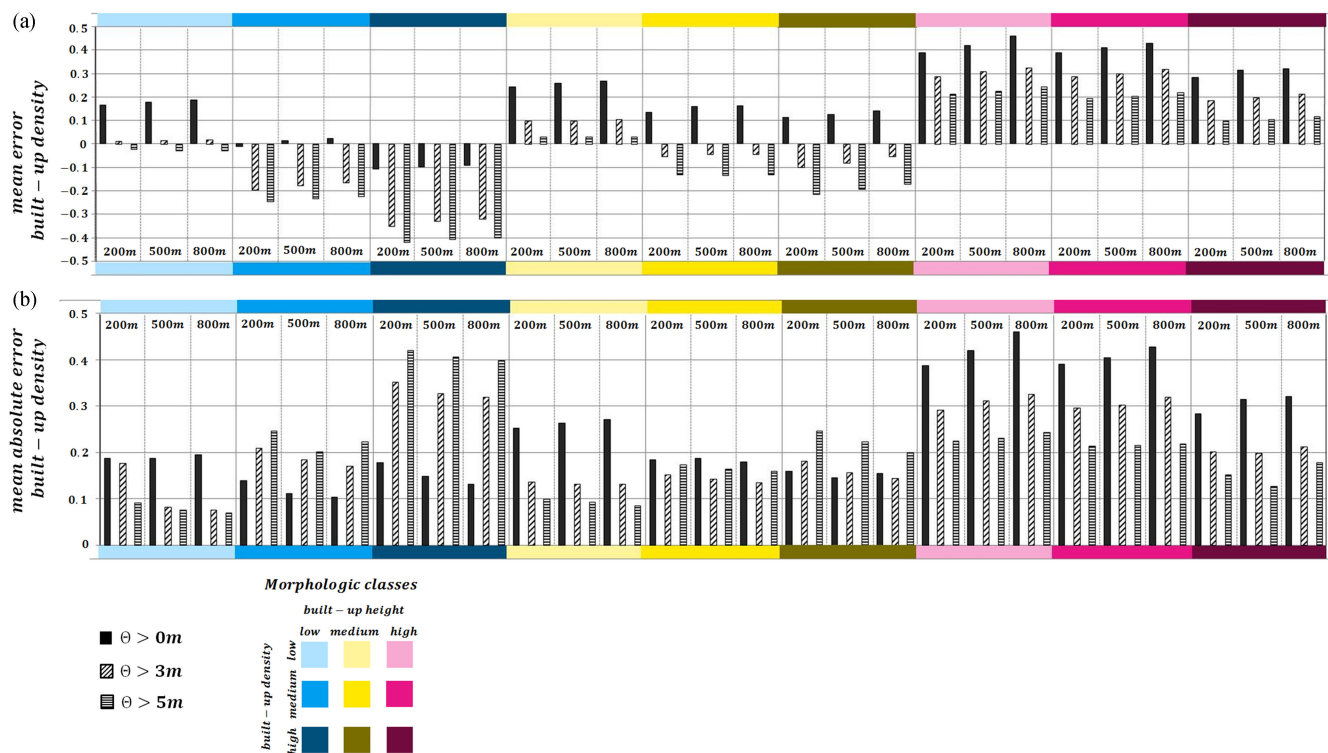


Fig. 7. Error measures for built-up density estimations. (a) ME and (b) MAE differentiated according to the nine morphologic classes and different values for the height threshold  $\Theta$  and the size of the grid cells.

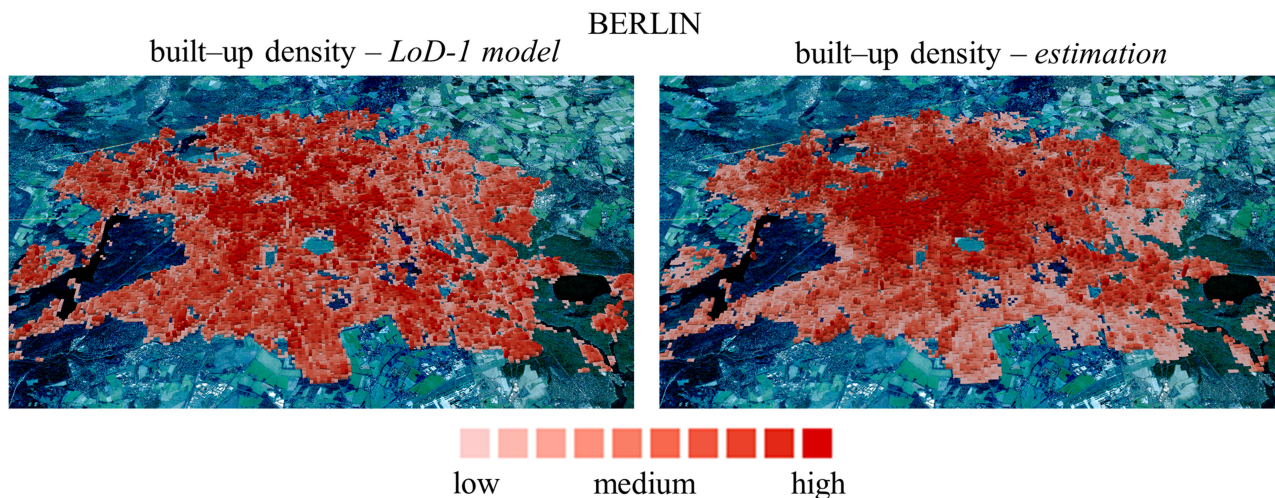


Fig. 8. Visualized built-up densities according to  $a = 200m$  ( $\Theta = 3m$  with respect to the *estimation*) for the example of Berlin, Germany. Color coding corresponds to deciles for the individual data sets and thus allows a relative spatial comparison; however, heights of bars correspond to absolute numerical values where numerical density values were superelevated 1000 times.

To illustrate further, Fig. 6 provides a visual comparison of estimated built-up heights and built-up heights derived from the building geometries of the LoD-1 model for the city of Berlin, Germany. In concordance with the previous results, it can be noted that estimated built-up heights are in tendency underestimated. However, the relative spatial pattern reflects the distribution of built-up heights with respect to the reference data set well. For instance, the urban core with *high* built-up heights is

equally well depicted as *low* built-up heights on the peripheral areas of the city.

### B. Accuracy of Built-Up Density

Accuracy of built-up density estimations differentiated according to the nine morphologic classes is provided in Fig. 7. Analogous to previous analysis, they are based on the reference

data sets of all ten considered cities. Results are presented as a function of different values for height threshold  $\Theta$  and size of the grid cells.

ME values [see Fig. 7(a)] show varying under- and overestimations with respect to the morphologic classes. Overestimations can be observed predominantly for areas which are characterized by *high* built-up heights. Those built-up structures can be primarily found in the central areas of the considered cities (i.e., the urban cores). Here, the estimations reveal an almost complete coverage by built-up structures while the reference data depict significant lower built-up densities. In contrast to that, underestimations can be noted mainly for areas which feature *low* built-up heights. Those built-up structures can be frequently found in the fringe of the agglomerations (i.e., residential areas at peripheral or suburban areas of the cities). The estimations assign very low built-up densities to those areas while the cadastral data, which is considered as ground truth information here, reveal significantly higher built-up densities. This relation can be dominantly attributed to the fact that intra-urban vegetation obscures underlying built-up structures when corresponding built-up heights are low. Comparable effects were also previously described in studies which aim to estimate the percentage of impervious surfaces based on remote sensing imagery (e.g., [52], [60]). Besides, for remaining morphologic classes, overestimations for progressive  $\Theta$  values and underestimations for restrictive  $\Theta$  values occur.

Regarding absolute error levels and in concordance with previous results, the MAE [see Fig. 7(b)] reveals lowest values for areas with *medium* built-up heights and largest values for structures with *high* built-up heights and *low* built-up densities (i.e., overestimations regarding the urban cores) as well as for areas with *low* built-up heights and *high* built-up densities (i.e., underestimations regarding residential areas at peripheral and suburban areas of the cities). Thus, also most favorable hyperparameters vary as a function of morphologic class: progressive  $\Theta$  values allow for reducing underestimations in areas with *low* built-up height and *high* built-up density, while restrictive  $\Theta$  values enable balancing overestimations for structures with *high* built-up height and *low* built-up density. However, for a moderately restrictive  $\Theta$  threshold (i.e.,  $\Theta = \{> 3\text{ m}\}$ ), viable built-up density estimations with deviations less than 20% are achieved for the majority of morphologic classes. An additional 10% deviation can be observed for the morphologic classes comprising *high* built-up heights and *low* and *medium* built-up densities as well as the class with *low* built-up heights and *high* built-up densities. In this setting and analogous to the built-up height estimations, errors levels frequently decrease slightly with an increasing size of the grid cells, since larger grid sizes are more likely to contain a mixture of structural types leveling local variations of density throughout urban morphology.

To illustrate the previous findings, Fig. 8 provides a visual comparison of estimated built-up densities and built-up densities derived from the building geometries of the LoD-1 model for the city of Berlin, Germany. The density estimations show an ideal decrease from the core to the fringe, whereby the LoD-1 model-based built-up densities also show highest densities in the urban core but are generally more spatially differentiated and

fragmented and feature higher levels in vast parts of the fringe areas.

### C. Morphologic Characterization

The built-up height and density estimations are finally combined within nine morphologic classes. Results for the capital cities are depicted in Fig. 9 with affiliated classification accuracy measures computed by comparing every single grid cell. Additionally, zoom-in windows for selected areas are shown. Results for the remaining cities are visualized in Fig. 10 with affiliated classification accuracy measures.

First, it can be noted that the overall morphologic structure of the cities is well reflected: They are dominantly characterized by a single or multiple urban core(s) and affiliated high built-up structures and lower built-up structures, which are also less densely arranged, in the peripheral parts. This structure primarily derives from a concentric, industrial city model with a defined center surrounded by a more or less complex halo of settlement structures with lower heights and densities and suburbs which ultimately turn into rural environments [61]. Thus, small-scale changes in the urban morphology are well reflected as can be seen from the classification outcome which is superimposed on the Sentinel-2 imagery in the zoom-in-windows of Fig. 9.

Regarding the class-specific classification accuracy measures, the user's and producer's accuracies reflect the findings from the previous analysis. While certain morphologic classes feature consistently both high user's and producer's accuracies, other morphologic classes mirror characteristic errors described in the evaluation of estimated built-up heights and densities before. Large omission errors (i.e., low producer's accuracies) can be observed for the class characterizing *low* built-up heights and *high* built-up densities with respect to the majority of cities (i.e., Berlin, London, Munich, Frankfurt, Stuttgart, and The Hague). Here, the underestimation of built-up densities in fringe areas prevents correct class assignments and corresponding areas are primarily allocated to the class with *low* built-up height and *low* built-up density. Likewise, large omission errors can be noticed for majority of cities for the two classes characterizing *high* built-up heights and *low* and *medium* built-up densities. Here, the general underestimation of built-up heights causes incorrect class assignments and corresponding areas are primarily allocated to the classes with *medium* built-up heights. Besides, some local sources of errors can be identified. As such, erroneous class assignments are present in cities where built-up structures in direct spatial vicinity to large water bodies exist (e.g., Amsterdam and Rotterdam). Although water bodies were pruned from further processing by inclusion of the TDM water mask (cf. Section III-D), a number of pixels still carry disproportional *high* height values in the UF-E model that lead to errors of commission for the class which describes *high* built-up heights and *high* and *medium* built-up densities. Nevertheless, global classification accuracy measures show OA values consistently exceeding 70% and  $\kappa$  statistics dominantly show substantial agreements (i.e.,  $\kappa$  statistic  $> 0.6$ ), which underlines the viability of the approach. As such, the produced data sets feature a great potential

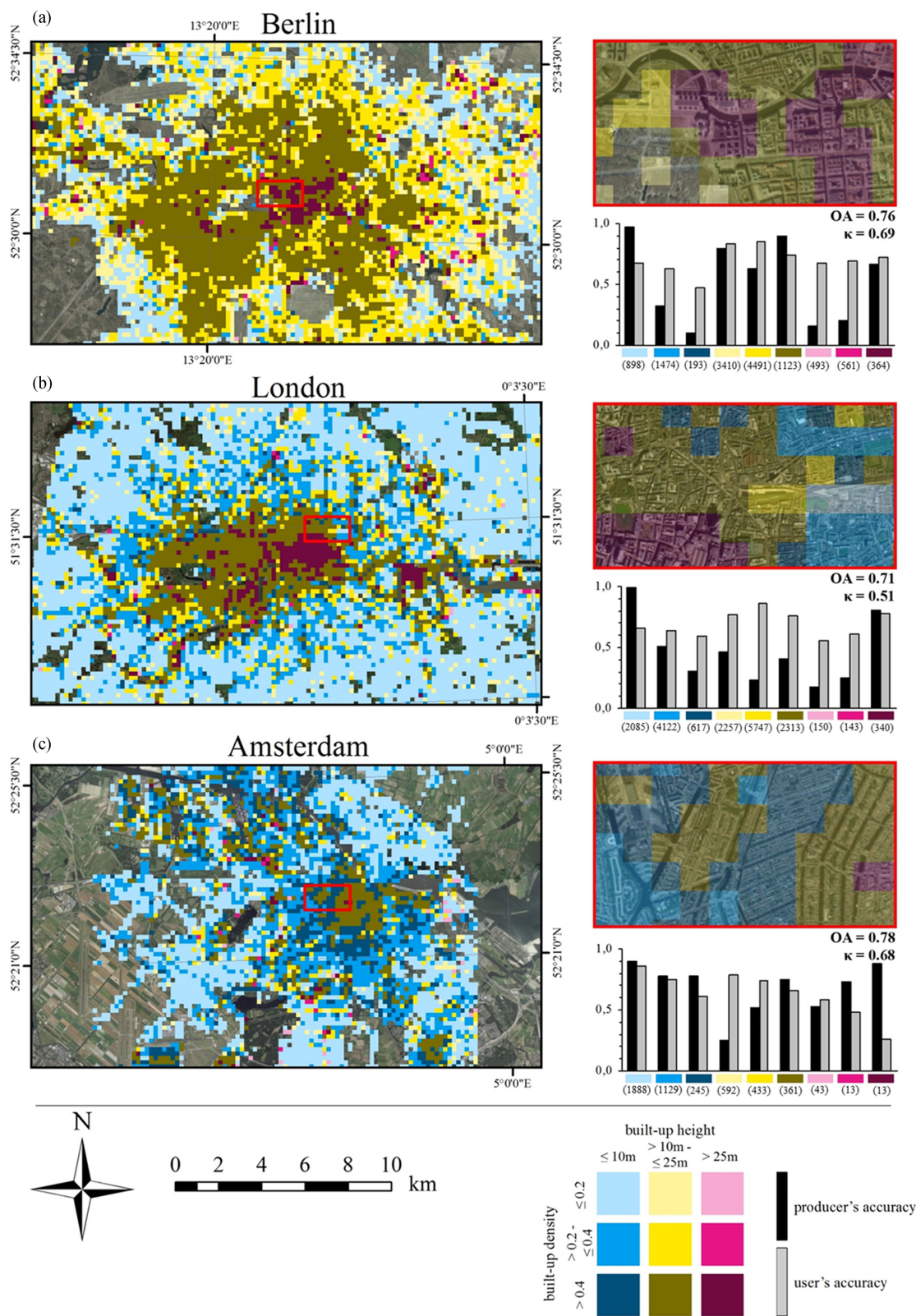


Fig. 9. Morphologic characterization for the capital cities (a) Berlin, (b) London, and (c) Amsterdam according to  $a = 200$  m; semi-transparent detailed views are superimposed on Sentinel-2 imagery. Ordinally weighted classification accuracy measures are also presented. Numbers in brackets below the producer's and user's accuracy bars indicate the numbers of grid cells per morphologic class based on the reference data which were used for computation of accuracy measures.

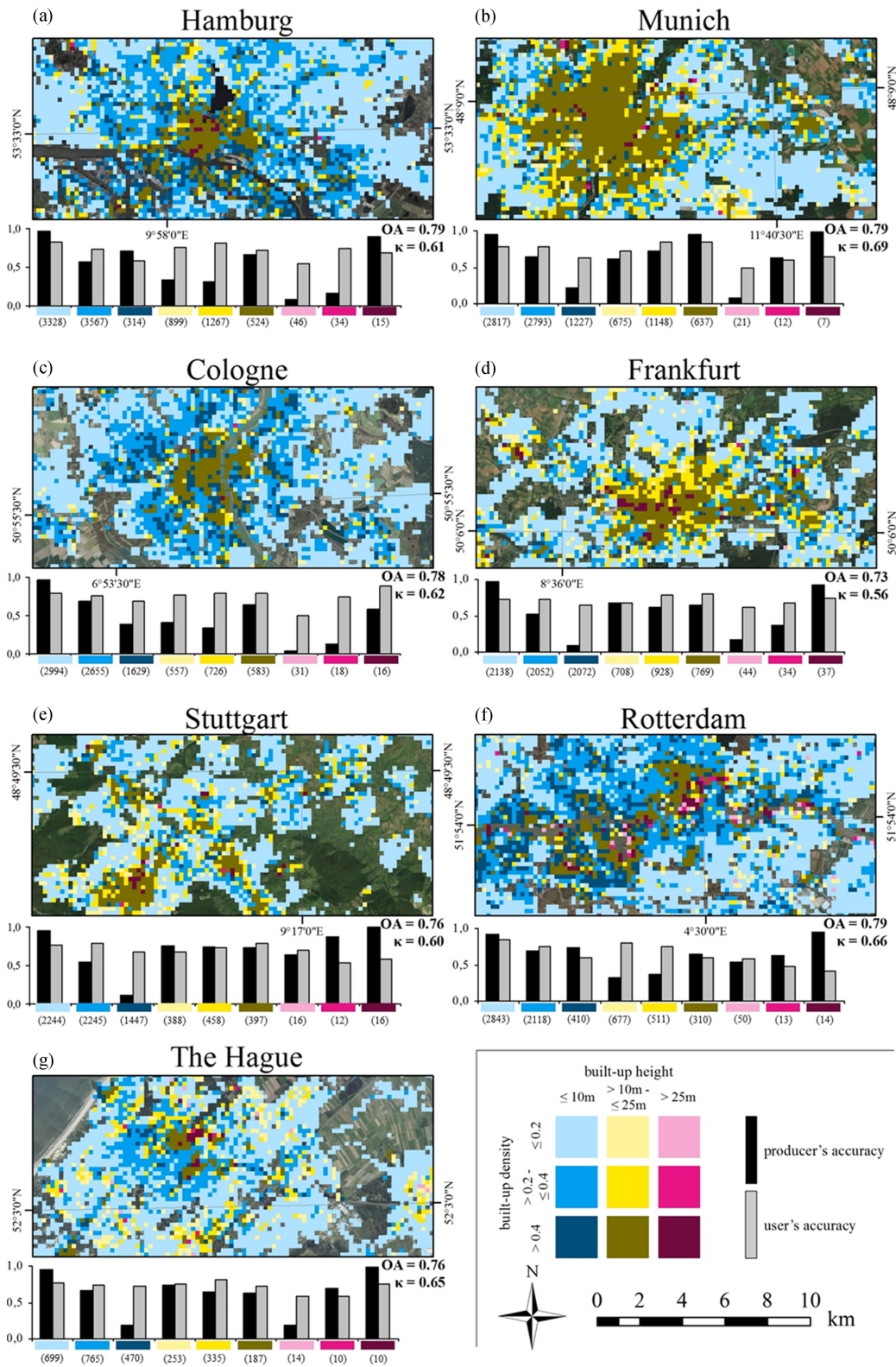


Fig. 10. Morphologic characterization for the cities (a) Hamburg, (b) Munich, (c) Cologne, (d) Frankfurt, (e) Stuttgart, (f) Rotterdam, and (g) The Hague according to  $a = 200$  m. Ordinally weighted classification accuracy measures are also presented. Numbers in brackets below the producer's and user's accuracy bars indicate the numbers of grid cells per morphologic class based on the reference data which were used for computation of accuracy measures.

for novel applications and objective comparative analysis between cities regarding the morphologic structure based on data with an unprecedented tradeoff between high spatial resolution and large-area coverage.

## V. CONCLUSION AND OUTLOOK

In this paper, we have proposed a novel workflow, which builds upon data from the TDM and Sentinel-2 imagery to characterize urban morphology for large areas in an automated manner. To this purpose, we rely on the GUF processor, which discriminates between “built-up” and “non-built-up” LC on a global scale while maintaining a high spatial detail. This binary description of built-up LC is extended by computing elevation information (i.e., UF-E model) from the TDM using a tailored filtering technique on the DSM. Derived information layers serve as input for a hierarchical classification scheme for intra-urban areas. The scheme foresees the delineation of intra-urban vegetation under consideration of information from the Sentinel-2 imagery. Subsequent to that, the UF-E model is used to further distinguish between “elevated built-up” and “residual intra-urban LC” in the remaining areas. Consequently, pixels of the class “elevated built-up” and affiliated elevation values from the UF-E model are used for mapping of built-up densities and heights and for creating the joint classes, which describe urban morphology.

Comparative evaluations with respect to cadastral data are obtained for settlement areas covering ten major cities in Germany, England, and the Netherlands. They uncover a systematic underestimation of built-up heights in relation to the reference data for all morphologic classes. However, error levels can be balanced by choosing appropriate hyperparameters of the approach. In this manner, built-up height estimations feature deviations of approximately one to two floors depending on the corresponding morphologic class and the relative spatial pattern reflects the distribution of built-up heights with respect to the reference data set well. The built-up densities show highest accuracies for areas with medium built-up heights. Lowest accuracies are obtained for structures with *high* built-up heights and *low* built-up densities (i.e., overestimations regarding the intra-urban cores) as well as for areas with *low* built-up heights and *high* built-up densities (i.e., underestimations regarding peripheral or suburban areas of the cities). Nevertheless, viable built-up density estimations with deviations of less than 20% are achieved for the majority of morphologic classes. In addition, the estimations reflect the general urban morphologic structure well by showing an ideal decrease from the core to the fringe of the agglomeration areas. Finally, regarding the actual morphologic characterization, ordinarily weighted global classification accuracy measures show OA values consistently exceeding 70% and  $\kappa$  statistics dominantly show substantial agreements.

The TDM and Sentinel-2 data offer the unique opportunity to assess urban morphology according to the proposed approach around the globe. However, for scientific applications the accessibility of the TDM data is currently limited to 100 000 km<sup>2</sup> per data proposal. To alleviate this limited accessibility, we aim

to develop an approach to substitute the TDM data. To this purpose, we will render the estimation of built-up density and height as a supervised learning problem [62]. In addition to that, we aim for reprocessing the Co-registered Single-look Slant-range Complex TDM data to establish a novel global DSM with enhanced geometric resolution properties using advanced signal processing algorithms [63], [64]. In addition, future work can also aim for refining accuracy of results by establishing empirically derived postprocessing models to align the estimations to reference data. This appears as a viable option since we found majority of deviations to be systematic (i.e., data inherent) and, thus, allow to be corrected for.

Overall, the envisaged data sets have the potential to substantially support and enable a broad range of area-wide applications as discussed in the introduction section. Besides, the TDM has been extended to generate an updated elevation model [49]. With it, monitoring of urban expansion could be extended from two-dimensional analysis [65] towards the quantification of change of built-up volumes over time. For the very first time, the extent of infill development and urban intensification would become observable for larger urban areas or even urban systems at national or supranational scales. Hence, valuable contributions to different fields of research are in prospect.

## APPENDIX

TABLE I  
LIST OF ABBREVIATIONS

DSM	digital surface model
DTM	digital terrain model
EO	earth observation
GUF	Global Urban Footprint
LC	land cover
LCZ	local climate zone
LOD-1	level of detail 1
ME	mean error
MAE	mean absolute error
NDSM	normalized DSM
NDVI	Normalized Difference Vegetation Index
OA	overall accuracy
SAR	synthetic aperture radar
TDM	TanDEM-X mission
UF-E	Urban Footprint – Elevation
VHR	very high spatial resolution

## REFERENCES

- [1] T. Leichte, C. Geiß, M. Wurm, T. Lakes, and H. Taubenböck, “Unsupervised change detection in VHR remote sensing imagery—An object-based clustering approach in a dynamic urban environment,” *Int. J. Appl. Earth Observ. Geoinform.*, vol. 54, pp. 15–27, 2017.
- [2] X. Huang, D. Wen, J. Li, and R. Qin, “Multi-level monitoring of subtle urban changes for the megacities of China using high-resolution multi-view satellite imagery,” *Remote Sens. Environ.*, vol. 196, pp. 56–75, 2017.

- [3] J. Graesser *et al.*, "Image based characterization of formal and informal neighborhoods in an urban landscape," *IEEE J. Sel. Topics Appl. Earth Observ. Remote Sens.*, vol. 5, no. 4, pp. 1164–1176, Aug. 2012.
- [4] H. Taubenböck *et al.*, "Delineation of central business districts in mega city regions using remotely sensed data," *Remote Sens. Environ.*, vol. 136, pp. 386–401, Sep. 2013.
- [5] S. Wu, X. Qiu, and L. Wang, "Population estimation methods in GIS and remote sensing: A review," *Int. J. Remote Sens.*, vol. 42, no. 1, pp. 80–96, 2005.
- [6] C. Geiß *et al.*, "Joint use of remote sensing data and volunteered geographic information for exposure estimation—Evidence from Valparaíso, Chile," *Natural Hazards*, vol. 86, pp. 81–105, 2017.
- [7] P. Rode, C. Keim, G. Robazza, P. Viejo, and J. Schofield, "Cities and energy: Urban morphology and residential heat-energy demand," *Environ. Planning B, Planning Design*, vol. 41, pp. 138–162, 2014.
- [8] M. Silva, V. Oliveira, and V. Leal, "Urban form and energy demand: A review of energy-relevant urban attributes," *J. Planning Lit.*, vol. 32, pp. 346–365, 2017.
- [9] C. Geiß *et al.*, "Remote sensing-based characterization of settlement structures for assessing local potential of district heat," *Remote Sens.*, vol. 3, no. 7, pp. 1447–1471, 2011.
- [10] T. R. Tooke *et al.*, "Mapping demand for residential building thermal energy services using airborne LiDAR," *Appl. Energy*, vol. 127, pp. 125–134, 2014.
- [11] D. Godoy-Shimizu *et al.*, "Energy use and height in office buildings," *Building Res. Inf.*, vol. 46, pp. 845–863, 2018.
- [12] C. Geiß and H. Taubenböck, "Remote sensing contributing to assess earthquake risk: From a literature review towards a roadmap," *Natural Hazards*, vol. 68, no. 1, pp. 7–48, Aug. 2013.
- [13] M. Pittore, M. Wieland, and K. Fleming, "Perspectives on global dynamic exposure modelling for geo-risk assessment," *Natural Hazards*, vol. 86, pp. 7–30, 2017.
- [14] B. Stone Jr. and M.O. Rodgers, "Urban form and thermal efficiency: How the design of cities influences the urban heat island effect," *J. Amer. Planning Assoc.*, vol. 67, no. 2, pp. 186–198, 2001.
- [15] R. Watkins, J. J. Palmer, and M. Kolokotroni, "Increased temperature and intensification of the urban heat island: Implications for human comfort and urban design," *Built Environ.*, vol. 33, pp. 85–96, 2007.
- [16] J. Heinzl and T. Kemper, "Automatic metric characterization of urban structure using building decomposition from very high resolution imagery," *Int. J. Appl. Earth Observ. Geoinform.*, vol. 35, pp. 151–160, 2015.
- [17] D. González-Aguilera *et al.*, "Automated urban analysis based on LiDAR-derived building models," *IEEE Trans. Geosci. Remote Sens.*, vol. 51, no. 3, pp. 1844–1851, Mar. 2013.
- [18] H. Taubenböck *et al.*, "The morphology of the Arrival City—A global categorization based on literature surveys and remotely sensed data," *Appl. Geogr.*, vol. 92, pp. 150–167, 2018.
- [19] G. Krieger *et al.*, "TanDEM-X: A satellite formation for high-resolution SAR interferometry," *IEEE Trans. Geosci. Remote Sens.*, vol. 45, no. 11, pp. 3317–3341, Nov. 2007.
- [20] M. Zink *et al.*, "TanDEM-X: The new global DEM takes shape," *IEEE Geosci. Remote Sens. Mag.*, vol. 2, no. 2, pp. 8–23, Jun. 2014.
- [21] M. Drusch *et al.*, "Sentinel-2: ESA's optical high-resolution mission for GMES operational services," *Remote Sens. Environ.*, vol. 120, pp. 25–36, May 2012.
- [22] C. Geiß *et al.*, "Assessment of seismic building vulnerability from space," *Earthquake Spectra*, vol. 30, no. 4, pp. 1553–1584, Nov. 2014.
- [23] M. Belgiu, I. Tomljenovic, T. Lampoltshammer, T. Blaschke, and B. Höfle, "Ontology-based classification of building types detected from airborne laser scanning data," *Remote Sens.*, vol. 6, no. 2, pp. 1347–1366, Feb. 2014.
- [24] S. Du *et al.*, "Semantic classification of urban buildings combining VHR image and GIS data: An improved random forest approach," *ISPRS J. Photogramm. Remote Sens.*, vol. 105, pp. 107–119, 2015.
- [25] C. Geiß *et al.*, "Estimation of seismic buildings structural types using multi-sensor remote sensing and machine learning techniques," *ISPRS J. Photogramm. Remote Sens.*, vol. 104, pp. 175–188, 2015.
- [26] M. Wurm, A. Schmitt, and H. Taubenböck, "Building types classification using shape-based features and linear discriminant functions," *IEEE J. Sel. Topics Appl. Earth Observ. Remote Sens.*, vol. 9, no. 5, pp. 1901–1912, May 2016.
- [27] C. Geiß *et al.*, "Multitask active learning for characterization of built environments with multisensor earth observation data," *IEEE J. Sel. Topics Appl. Earth Observ. Remote Sens.*, vol. 10, no. 12, pp. 5583–5597, Dec. 2017.
- [28] U. Heiden, W. Heldens, S. Roessner, K. Segl, T. Esch, and A. Mueller, "Urban structure type characterization using hyperspectral remote sensing and height information," *Landsc. Urban Plann.*, vol. 105, pp. 361–375, 2012.
- [29] C. Geiß, M. Jilge, T. Lakes, and H. Taubenböck, "Estimation of seismic vulnerability levels of urban structures with multisensor remote sensing," *IEEE J. Sel. Topics Appl. Earth Observ. Remote Sens.*, vol. 9, no. 5, pp. 1913–1936, May 2016.
- [30] P. Soille, *Morphological Image Analysis: Principles and Applications*. Heidelberg, Germany: Springer, 2004.
- [31] T. Zhang, X. Huang, D. Wen, and J. Li, "Urban building density estimation from high-resolution imagery using multiple features and support vector regression," *IEEE J. Sel. Topics Appl. Earth Observ. Remote Sens.*, vol. 10, no. 7, pp. 3265–3280, Jul. 2017.
- [32] D. Luebke, B. Watson, J. D. Cohen, M. Reddy, and A. Varshney, *Level of Detail for 3D Graphics*. San Francisco, CA, USA: Elsevier, 2002.
- [33] A. Krehl, S. Siedentop, H. Taubenböck, and M. Wurm, "A comprehensive view on urban spatial structure: Urban density patterns of German city regions," *Int. J. Geo-Inf.*, vol. 5, pp. 1–21, 2016.
- [34] H. Taubenböck *et al.*, "The physical density of the city – Deconstruction of the delusive density measure with evidence from two European megacities," *ISPRS Int. J. Geo-Inf.*, vol. 5, no. 11, 2016, doi: [10.3390/ijgi5110206](https://doi.org/10.3390/ijgi5110206).
- [35] C. Berger *et al.*, "Multi-modal and multi-temporal data fusion: Outcome of the 2012 GRSS data fusion contest," *IEEE J. Sel. Topics Appl. Earth Observ. Remote Sens.*, vol. 6, no. 3, pp. 1324–1340, Jun. 2013.
- [36] I. D. Stewart and T. R. Oke, "Local climate zones for urban temperature studies," *Bull. Amer. Meteorol. Soc.*, vol. 93, no. 12, pp. 1879–1900, Dec. 2012.
- [37] B. Bechtel and C. Daneke, "Classification of local climate zones based on multiple earth observation data," *IEEE J. Sel. Topics Appl. Earth Observ. Remote Sens.*, vol. 5, no. 4, pp. 1191–1202, Aug. 2012.
- [38] B. Bechtel, "Mapping local climate zones for a worldwide database of the form and function of cities," *ISPRS Int. J. Geo-Inf.*, vol. 4, pp. 199–219, 2015.
- [39] C. Geiß, M. Wurm, and H. Taubenböck, "Towards large-area morphologic characterization of urban environments using the TanDEM-X mission and Sentinel-2," in *Proc. 2017 Joint Urban Remote Sens. Event*, Dubai, UAE, 2017, pp. 1–4, doi: [10.1109/JURSE.2017.7924543](https://doi.org/10.1109/JURSE.2017.7924543).
- [40] T. Esch *et al.*, "Breaking new ground in human settlements from space—The Global Urban Footprint," *ISPRS J. Photogramm. Remote Sens.*, vol. 134, pp. 30–42, 2017.
- [41] M. Klotz, T. Kemper, C. Geiß, T. Esch, and H. Taubenböck, "How good is the map? A multi-scale cross-comparison framework for global settlement layers: Evidence from Central Europe," *Remote Sens. Environ.*, vol. 178, pp. 191–212, 2016.
- [42] C. Geiß, M. Wurm, M. Breunig, A. Felbier, and H. Taubenböck, "Normalization of TanDEM-X DSM data in urban environments with morphological filters," *IEEE Trans. Geosci. Remote Sens.*, vol. 53, no. 8, pp. 4348–4362, Aug. 2015.
- [43] B. Wessel, "TanDEM-X ground segment – DEM products specification document," EOC, DLR, Oberpfaffenhofen, Germany, Public Document TD-GS-PS-0021, Issue 3.1, 2016. [Online]. Available: <https://tandemx-science.dlr.de/>
- [44] J. W. Rouse, R. H. Haas, J. A. Schell, and D. W. Deering, "Monitoring vegetation systems in the great plains with ERTS," in *Proc. 3rd Earth Resour. Technol. Satell.-1 Symp.*, 1974, pp. 309–317.
- [45] J. Schreyer, C. Geiß, and T. Lakes, "TanDEM-X for large-area modeling of Urban vegetation height: Evidence from Berlin, Germany," *IEEE J. Sel. Topics Appl. Earth Observ. Remote Sens.*, vol. 9, no. 5, pp. 1876–1887, May 2016.
- [46] T. Esch, M. Thiel, A. Schenk, A. Roth, A. Müller, and S. Dech, "Delineation of urban footprints from TerraSAR-X data by analyzing speckle characteristics and intensity information," *IEEE Trans. Geosci. Remote Sens.*, vol. 48, no. 2, pp. 905–916, Feb. 2010.
- [47] N. Otsu, "A threshold selection method from gray-level histograms," *IEEE Trans. Syst., Man, Cybern.*, vol. SMC-9, no. 1, pp. 62–66, Jan. 1979.
- [48] B. Wessel *et al.*, "Accuracy assessment of the global TanDEM-X Digital Elevation Model with GPS data," *ISPRS J. Photogramm. Remote Sens.*, vol. 139, pp. 171–182, 2018.
- [49] P. Rizzoli *et al.*, "Generation and performance assessment of the global TanDEM-X digital elevation model," *ISPRS J. Photogramm. Remote Sens.*, vol. 132, pp. 119–139, 2017.
- [50] European Space Agency (ESA) - Science Toolbox Exploitation Platform, Sentinel Application Platform. [Online]. Available: <http://step.esa.int/main/toolboxes/snap/>. Accessed on: May 16, 2018.
- [51] European Space Agency (ESA) - Sen2Cor. [Online]. Available: <http://step.esa.int/main/third-party-plugins-2/sen2cor/>. Accessed on: May 16, 2018.
- [52] P. Leinenkugel, T. Esch, and C. Künzer, "Settlement detection and impervious surface estimation in the Mekong Delta using optical and SAR remote sensing data," *Remote Sens. Environ.*, vol. 115, pp. 3007–3019, 2011.

- [53] M. Wurm, P. d'Angelo, P. Reinartz, and H. Taubenböck, "Investigating the applicability of cartosat-1 DEMs and topographic maps to localize large-area urban mass concentrations," *IEEE J. Sel. Topics Appl. Earth Observ. Remote Sens.*, vol. 7, no. 10, pp. 4138–4152, Oct. 2014.
- [54] ESRI Nederland – Community Map Contributors. [Online]. Available: <http://www.arcgis.com/apps/Viewer/index.html?appid=2e4c2b5b127a447e94997bbffd41b93e>. Accessed on: May 16, 2018.
- [55] D. Shepard, "A two-dimensional interpolation function for irregularly spaced data," in *Proc. 23rd ACM Nat. Conf.*, Aug. 27–29, 1968, pp. 517–524.
- [56] C. J. Willmott and K. Matsuura, "Advantages of the mean absolute error (MAE) over the root mean square error (RMSE) in assessing average model performance," *Clim. Res.*, vol. 30, pp. 79–82, 2005.
- [57] J. S. Cardoso and R. Sousa, "Measuring the performance of ordinal classification," *Int. J. Pattern Recognit. Artif. Intell.*, vol. 25, no. 8, pp. 1173–1195, 2011.
- [58] G. M. Foody, "Thematic map comparison: Evaluating the statistical significance of differences in classification accuracy," *Photogramm. Eng. Remote Sens.*, vol. 50, no. 5, pp. 627–633, 2004.
- [59] M. Wurm, H. Taubenböck, M. Schardt, T. Esch, and S. Dech, "Object-based image information fusion using multisensor earth observation data over urban areas," *Int. J. Image Data Fusion*, vol. 2, no. 2, pp. 121–147, 2011.
- [60] T. Esch *et al.*, "Large-area assessment of impervious surface based on integrated analysis of single-date Landsat-7 images and geospatial vector data," *Remote Sens. Environ.*, vol. 113, pp. 1678–1690, 2009.
- [61] H. Taubenböck, I. Standfuß, M. Wurm, A. Krehl, and S. Siedentop, "Measuring morphological polycentricity—A comparative analysis of urban mass concentrations using remote sensing data," *Comput., Environ. Urban Syst.*, vol. 64, pp. 42–56, 2017.
- [62] C. Geiß, H. Schrade, and H. Taubenböck, "Boosted machine learning ensemble regression with decision fusion strategy for mapping built-up height and built-up density with Openstreetmap data and Sentinel-2 imagery," in *Proc. 5th EARSel Joint Workshop "Urban Remote Sens. Challenges Solutions"*, Bochum, Germany, Sep. 24–26, 2018, p. 1.
- [63] G. Baier *et al.*, "A nonlocal InSAR filter for high-resolution DEM generation from TanDEM-X interferograms," *IEEE Trans. Geosci. Remote Sens.*, vol. 56, no. 11, pp. 6469–6483, 2018.
- [64] X. X. Zhu, G. Baier, M. Lachaise, Y. Shi, F. Adam, and R. Bamler, "Potential and limits of non-local means InSAR filtering for TANDEM-X high-resolution DEM generation," *Remote Sens. Environ.*, vol. 218, pp. 148–161, 2018.
- [65] H. Taubenböck, T. Esch, A. Felbier, M. Wiesner, A. Roth, and S. Dech, "Monitoring urbanization in mega cities from space," *Remote Sens. Environ.*, vol. 117, pp. 162–176, 2012.



**Christian Geiß** (M'15) received the M.Sc. degree in applied geoinformatics from the Paris Lodron University of Salzburg, Salzburg, Austria, in 2010, and the Ph.D. degree (*Dr. rer. nat.*) from the Humboldt University of Berlin, Berlin, Germany, in 2014.

Since 2010, he has been with the German Remote Sensing Data Center (DFD), German Aerospace Center (DLR), Weßling, Germany. In 2017, he was also with the Cambridge University Centre for Risk in the Built Environment (CURBE), University of Cambridge, Cambridge, U.K., as a Visiting Scholar. His

current research interests include the development of machine learning methods for the interpretation of earth observation data, multimodal remote sensing of the built environment, exposure and vulnerability assessment in the context of natural hazards, and techniques for automated damage assessment after natural disasters.



**Tobias Leichtle** received the B.Sc. degree in geography from the Ludwig-Maximilians University of Munich, Munich, Germany, in 2009, and the M.Sc. degree in geospatial technologies from Karl-Franzens University and the Technical University of Graz, Austria, in 2013. He is currently working toward the Ph.D. degree with the Humboldt University of Berlin, Berlin, Germany.

From 2013 to 2018, he was a Research Associate at the Company for Remote Sensing and Environmental Research (SLU), Munich. In 2019, he joined the German Remote Sensing Data Center (DFD), German Aerospace Center (DLR), Weßling, Germany. His current research interests include the development of machine learning methods for information extraction from multimodal earth observation data, change detection in VHR remote sensing imagery as well as the analysis of associated transformations of urban structure in the context of urban geography.



**Michael Wurm** received the Diploma degree (*Mag. rer. nat.*) in geography with a specialization in remote sensing, GIS, and spatial research from the University of Graz, Graz, Austria, in 2007, and the Ph.D. degree (*Dr. rer. nat.*) in surveying and geoinformation from the Graz University of Technology, Graz, in 2013.

He was with the Institute of Digital Image Processing, Joanneum Research, Graz, in 2007. In 2008, he joined the University of Würzburg, Germany, where he was engaged in the integration of earth observation data into social sciences and urban remote sensing as

well as urban vulnerability research. In 2011, he joined the German Remote Sensing Data Center (DFD), German Aerospace Center (DLR), Weßling, Germany, where he is involved in conducting research on urban geography, with a particular interest in urban structure analyses and urban morphology. Since 2013, he has been a Lecturer with the University of Graz.



**Patrick Aravena Pelizari** received the M.Sc. degree in physical geography/environmental systems from Ludwig-Maximilians University, Munich, Germany, in 2013.

In 2013, he joined the German Remote Sensing Data Center (DFD), German Aerospace Center (DLR), Weßling, Germany, as a Research Associate, where he has been contributing to several research projects in the fields of humanitarian relief and natural disasters management focusing on the use of machine learning techniques to extract related information from multi-sensoral remote sensing data as well as on subsequent geostatistical analyses. His current research addresses method development to assess the vulnerability of built environments to natural hazards integrating earth observation as well as geodata from multiple sources. Currently, his particular interest

in this context is the use of deep learning algorithms.



**Ines Standfuß** received the Diploma (Dipl.-Ing.) in spatial planning from the Technical University of Dortmund, Dortmund, Germany, in 2012, and the M.Sc. degree in geography with a focus on geomatics from Ruhr-University Bochum, Bochum, Germany, in 2015. She is currently working toward the Ph.D. degree with the German Remote Sensing Data Center (DFD), German Aerospace Center (DLR), Weßling, Germany.

Her current research interests include the influence of the natural and built environment on behavior and

movement of birds.



**Xiao Xiang Zhu** (S'10–M'12–SM'14) received the M.Sc. degree, the Dr.-Ing. Degree, and the “Habilitation” degree in the field of signal processing from the Technical University of Munich (TUM), Munich, Germany, in 2008, 2011, and 2013, respectively.

She is currently a Professor of Signal Processing in Earth Observation ([www.sipeo.bgu.tum.de](http://www.sipeo.bgu.tum.de)) at the Technical University of Munich (TUM) and German Aerospace Center (DLR), Weßling, Germany; the Head of the Department “EO Data Science” at DLR’s Earth Observation Center; and the Head of

the Helmholtz Young Investigator Group “SIPEO” at DLR and TUM. Since 2019, she has been co-coordinating the Munich Data Science Research School ([www.mu-ds.de](http://www.mu-ds.de)). She is also leading the Helmholtz Artificial Intelligence Cooperation Unit (HAICU) – Research Field “Aeronautics, Space and Transport.” She was a Guest Scientist or Visiting Professor at the Italian National Research Council (CNR-IREA), Naples, Italy, in 2009; Fudan University, Shanghai, China, in 2014; the University of Tokyo, Tokyo, Japan, in 2015; and the University of California, Los Angeles, CA, USA, in 2016. Her current research interests include remote sensing and earth observation, signal processing, machine learning, and data science, with a special application focus on global urban mapping.

Dr. Zhu is a member of Young Academy (Junge Akademie/Junges Kolleg) at the Berlin-Brandenburg Academy of Sciences and Humanities and the German National Academy of Sciences Leopoldina and the Bavarian Academy of Sciences and Humanities. She is an Associate Editor of the IEEE TRANSACTIONS ON GEOSCIENCE AND REMOTE SENSING.



**Emily So** received the Ph.D. degree in civil engineering from the Department of Architecture, University of Cambridge, Cambridge, U.K., in 2009.

She is a Senior Lecturer with the Department of Architecture, University of Cambridge. She was a Senior Geotechnical Engineer at Arup and has most recently finished a two-year appointment at the U.S. Geological Survey as a Mendenhall Fellow. Her research has led to improved understanding of the relationship between death and injury following earthquakes. Her work and the international contacts

developed have been instrumental in establishing an international network on disaster casualties. She has actively engaged with earthquake-affected communities in different parts of the world, focusing on applying her work toward making real-world improvements in seismic safety. She has been involved in interdisciplinary and international collaboration through her work with the UK Earthquake Field Investigation Team (EEFIT) and the Global Earthquake Model (GEM) and is actively participating in the international debate on the way forward for earthquake risk mitigation. Her current research interests include casualty estimation in earthquake loss modeling.

Dr. So is the 2010 Shah Family Innovation Prize winner, an award given annually by the Earthquake Engineering Research Institute (EERI) to promising young practitioners or academics. She is a Chartered Civil Engineer. She is the Director of Studies and Fellow in Architecture at Magdalene College and a Director of Cambridge Architectural Research Ltd.



**Stefan Siedentop** received the Diploma in spatial planning and the Ph.D. degree (Dr.-Ing.) from the Technical University of Dortmund, Dortmund, Germany, in 1994 and 2001, respectively.

Since 2013, he has been a Professor of Urban Development at the Technical University of Dortmund and the Director of the ILS-Research Institute for Regional and Urban Development, Dortmund, Germany. His current research interests include issues of urban spatial structure, land use change, urban infrastructure, and demographics.



**Thomas Esch** received the Diploma in applied physical geography from the University of Trier, Trier, Germany, in 2003, and the Ph.D. degree in physical geography and remote sensing from the University of Würzburg, Germany, in 2006.

He is a Leader of the team “Smart Cities and Spatial Development” and Project Manager at the German Remote Sensing Data Center (DFD), German Aerospace Center (DLR), Weßling, Germany, where since 2008, he has been with the Earth Observation Center (EOC), where he is engaged in conducting

research into remote sensing applications for urban and spatial planning, sustainable development, land management, energy efficiency, and urban microclimate. He has coordinated and participated in more than 20 national and international projects (i.a., Global Urban Footprint, Urban Thematic Exploitation Platform). In the Group on Earth Observation (GEO), he is the Co-Lead of task GI-17 “Global Urban Observation and Information” and member of the Steering Committee of the “Human Planet Initiative.” He is also an Assistant Lecturer at the Hochschule für Technik, Stuttgart, Germany. His research activities are documented by contributions to more than 35 peer-reviewed journal publications, 25 book chapters, and 170 conferences and workshops.



**Hannes Taubenböck** received the Diploma in geography from the Ludwig-Maximilians Universität München, Munich, Germany, in 2004, and the Ph.D. degree (*Dr. rer. nat.*) in geography from the Julius Maximilian’s University of Würzburg, Würzburg, Germany, in 2008.

In 2005, he joined the German Remote Sensing Data Center (DFD), German Aerospace Center (DLR), Weßling, Germany. After a postdoctoral research phase with the University of Würzburg (2007–2010), he returned in 2010 to DLR–DFD as a Scientific Employee. In 2013, he became the Head of the “City and Society” team.

In 2019, he habilitated at the University of Würzburg in Geography. His current research interests include urban remote sensing topics, from the development of algorithms for information extraction to value adding to classification products for findings in urban geography.